

Pair production of neutralinos via photon-photon collisions *

Zhou Fei^b, Ma Wen-Gan^{a,b}, Jiang Yi^b and Han Liang^b^aCCAST (World Laboratory), P.O.Box 8730, Beijing 100080, China.^bDepartment of Modern Physics, University of Science and Technology of China (USTC), Hefei, Anhui 230027, China.**Abstract**

We investigated the production of neutralino pairs via photon-photon collisions in the minimal supersymmetric model(MSSM) at future linear colliders. The numerical analysis of their production rates is carried out in the mSUGRA scenario. The results show that this cross section can reach about 18 femto barn for $\tilde{\chi}_1^0\tilde{\chi}_2^0$ pair production and 9 femto barn for $\tilde{\chi}_2^0\tilde{\chi}_2^0$ pair production with our chosen input parameters.

PACS number(s): 14.80.Ly, 12.15.Ji, 12.60.Jv

*The project supported by National Natural Science Foundation of China

1. Introduction

In the supersymmetric theory[1], proper electroweak symmetry breaking induces the right properties of the lightest supersymmetric particle (LSP) to be a natural candidate for weak-interacting cold dark matter, which can explain many astrophysical observations[2]. The minimal supersymmetric standard model(MSSM)[1] predicts that there exists an absolutely stable LSP. Most often the LSP in the MSSM theory is the lightest Majorana fermionic neutralino $\tilde{\chi}_1^0$. Therefore the production of the lightest neutralino $\tilde{\chi}_1^0$ and the second lightest neutralino $\tilde{\chi}_2^0$ may be studied at present and future experiments and the detailed study of the neutralino sector will help us to determine which kind of the supersymmetric models really exists in nature. In the MSSM, the physical neutralino mass eigenstates $\tilde{\chi}_i^0$ ($i = 1 \sim 4$) are the combinations of the neutral gauginos(\tilde{B}, \tilde{W}^3) and the neutral higgsinos($\tilde{H}_1^0, \tilde{H}_2^0$). In the two-component fermion fields $\psi_j^0 = (-i\lambda', -i\lambda^3, \psi_{H_1^0}, \psi_{H_2^0})$ [3], where λ' is the bino and λ^3 is the neutral wino, the neutralino mass matrix in the Lagrangian is given by

$$\mathcal{L}_M = -\frac{1}{2}(\psi^0)^T Y \psi^0 + h.c., \quad (1.1)$$

where the matrix Y reads

$$Y = \begin{pmatrix} M_1 & 0 & -m_Z \sin \theta_W \cos \beta & m_Z \sin \theta_W \sin \beta \\ 0 & M_2 & m_Z \cos \theta_W \cos \beta & -m_Z \cos \theta_W \sin \beta \\ -m_Z \sin \theta_W \cos \beta & m_Z \cos \theta_W \cos \beta & 0 & -\mu \\ m_Z \sin \theta_W \sin \beta & -m_Z \cos \theta_W \sin \beta & -\mu & 0 \end{pmatrix} \quad (1.2)$$

In the above equation, the neutralino mass matrix is related to four unknown parameters, namely μ , M_2 , M_1 and $\tan \beta = v_2/v_1$, ratio of the vacuum expectation values of the two Higgs fields. μ is the supersymmetric Higgs-boson-mass parameter and M_2 and M_1 are the gaug-

ino mass parameters associated with the $SU(2)$ and $U(1)$ subgroups, respectively. In CP-noninvariant theories, M_1 , M_2 and higgsino mass parameter μ can be complex. However, M_2 can be real and positive without loss of generality by reparametrization of the fields. In this work we shall investigate neutralino pair production in framework of the MSSM while ignoring CP-violation and taking M_1 and μ as being real. The matrix Y is symmetric and can be diagonalized by one unitary matrix N such that $N_D = N^* Y N^+ = \text{diag}(m_{\tilde{\chi}_1^0}, m_{\tilde{\chi}_2^0}, m_{\tilde{\chi}_3^0}, m_{\tilde{\chi}_4^0})$ in order of $m_{\tilde{\chi}_1^0} \leq m_{\tilde{\chi}_2^0} \leq m_{\tilde{\chi}_3^0} \leq m_{\tilde{\chi}_4^0}$. Then the two-component mass eigenstates can be

$$\chi_i^0 = N_{ij} \psi_j^0, \quad i, j = 1, \dots, 4. \quad (1.3)$$

The proper four-component mass eigenstates are defined in terms of two-component fields as

$$\tilde{\chi}_i^0 = \begin{pmatrix} \chi_i^0 \\ \tilde{\chi}_i^0 \end{pmatrix} \quad (i = 1, \dots, 4), \quad (1.4)$$

and the mass term becomes

$$\mathcal{L}_m = -\frac{1}{2} \sum_i \tilde{M}_i \tilde{\chi}_i^0 \tilde{\chi}_i^0, \quad (1.5)$$

where \tilde{M}_i 's are the diagonal elements of N_D .

The future e^+e^- Linear Colliders(LC) are designed to give facilities for e^+e^- , $\gamma\gamma$ and other collisions at the energy of $500 \sim 2000 \text{ GeV}$ with a luminosity of the order $10^{33} \text{ cm}^{-2} \text{ s}^{-1}$ [4]. For example, the proposed TESLA collider is known as a powerful tool for exploration the multi-hundred GeV scale[5]. Different options of this machine, namely, e^+e^- , $\gamma\gamma$, γe and e^-e^- are complementary to each other and will add essential new information to that obtained from the LHC. Its annual (10^7 s) $\gamma\gamma$ luminosity will be about $10 - 30 \text{ fb}^{-1}$ (in the

high energy peak) with possible upgrade of luminosity by one order of magnitude. Searching for supersymmetric particles and determining their properties are one of the main tasks at future LC. In detecting the existence of neutralinos, both e^+e^- and $\gamma\gamma$ collisions have clearer background than hadron collisions, but $\gamma\gamma$ collision at LC would have distinct advantage over the situation of LC operating in the e^+e^- collision mode, where the resonant effects of Higgs bosons can be observed only at some specific center of mass energy ranges of the machine and the possible s-channel suppression would generally reduce the cross section of neutralino pair production. Because of the continuous c.m.s energy distribution of the colliding photons back-scattered by e^- and e^+ beams, the intermediate resonant effects of Higgs bosons could enhance the neutralino pair production rate over a rather wide colliding energy range at electron-positron colliders.

So far there is no experimental evidence for neutralinos at CERN LEP2. They only set lower bound on the lightest neutralino mass $m_{\tilde{\chi}_1^0}$. Recent experimental reports presented that the mass of the lightest neutralino may be larger than $32.5 GeV$ [6] and the lower limit of the chargino mass is $76.8 GeV$ [7]. The direct neutralino pair productions at the CERN Large Hadron Collider (LHC) are studied in references [8][9][10]. The production of neutralino pair can be produced also at the LC machine operating in both e^-e^+ and $\gamma\gamma$ collision modes. Recently, it has been found that the $\tilde{\chi}_1^0\tilde{\chi}_2^0$ production rate in e^+e^- collision mode can reach several hundred femto barn[11].

In this paper we investigate the potential of direct neutralino pair production at the LC operating in photon-photon collision mode in framework of the MSSM with complete one-

loop Feynman diagrams. The numerical calculation will be illustrated in the CP-conserving mSUGRA scenario with five input parameters, namely $m_{1/2}$, m_0 , A_0 , μ and $\tan\beta$, where $m_{1/2}$, m_0 and A_0 are the universal gaugino mass, scalar mass at GUT scale and the trilinear soft breaking parameter in the superpotential respectively. From these five parameters, all the masses and couplings of the model are determined by evolution from the GUT scale down to the low electroweak scale [12]. The paper is organized as follows: In section 2, we give calculations of the neutralino pair production at the LC operating in photon-photon collision mode. In section 3, we discuss the numerical results of the cross sections. A short summary is presented in section 4. Finally the explicit expressions of form factors for s-channel diagrams are listed.

2. The Calculation of $e^+e^- \rightarrow \gamma\gamma \rightarrow \tilde{\chi}_i^0 \tilde{\chi}_j^0$

Neutralinos can be produced at e^+e^- colliders, either in diagonal or in mixed pairs. In this section we calculate the processes

$$e^+e^- \rightarrow \gamma\gamma \rightarrow \tilde{\chi}_i^0 \tilde{\chi}_j^0, \quad (i = 1, 2, j = 2).$$

The generic Feynman diagrams contributing to the subprocess $\gamma\gamma \rightarrow \tilde{\chi}_i^0 \tilde{\chi}_j^0$ in the MSSM at one-loop level are depicted in Fig.1, where the exchange of incoming photons in Fig.1(a.1 ~ 6), Fig.1(b.5) and Fig.1(c.1 ~ 4) are not shown. Fig.1(a.1 ~ 6) are box diagrams. Fig.1(b.1 ~ 5) are quartic interaction diagrams. Fig.1(c.1 ~ 3) represent triangle diagrams. The Fig.1(b.3 ~ b.5), (c.1 ~ 3) are also called s-channel diagrams. The Feynman diagrams in Fig.1 include the loops of quarks(U,D), squarks (\tilde{U}, \tilde{D}), leptons(E), sleptons(\tilde{E}) of three

generations, charginos, W^+ boson, charged ghost particles, charged Higgs boson and goldstone. Due to the Yukawa couplings strength, the contributions from the loop diagrams of the third generation quarks and squarks are more important than those from other diagrams. Here we should mention two points: (1) There is no diagram with a triangle squark(slepton) loop coupling with an A^0 or G^0 boson in Fig.1, because the vertices of $A^0(G^0) - \tilde{q} - \tilde{q}$ vanish[13]. (2) Our calculation shows that the Feynman diagrams involving quartic vertices $\gamma - h^0 - G^+(H^+) - G^-(H^-)$ and $\gamma - H^0 - G^+(H^+) - G^-(H^-)$, which have similar structure to Fig.1(b.5), have no contribution to the cross section, therefore omitted in figure 1. The Z^0 boson intermediated s-channel diagrams similar to the diagrams of Fig.1(b.3) \sim (b.5), Fig.1(c.1) \sim (c.3) are not plotted in Fig.1 either, since they cannot contribute to the cross section. For this result there are two reasons: (1) The CP-odd scalar component of the Z^0 boson does not couple to the invariant CP-even $\tilde{\chi}_i^0 \tilde{\chi}_j^0$ state. (2) The vector component of the Z^0 boson wave function does not couple to the initial $\gamma\gamma$ state as the result of the Landau-Yang theorem.

Since there is no tree level diagram for the neutralino pair production via photon-photon collisions, the calculation for this process can be simply carried out by summing all unrenormalized reducible and irreducible one-loop diagrams and the results will be finite and gauge invariant. In this work, we perform the calculation in the 't Hooft-Feynman gauge, and take the CKM matrix as identity.

We denote the reaction of neutralino pair production via photon-photon collisions as:

$$\gamma(p_1, \mu)\gamma(p_2, \nu) \longrightarrow \tilde{\chi}_i^0(k_1)\tilde{\chi}_j^0(k_2), \quad (i = 1, 2, j = 2). \quad (2.1)$$

where p_1 , p_2 and k_1 , k_2 denote the four momenta of the incoming photons and outgoing neutralinos, respectively. In calculation of the amplitude, one should note that there should be a relative sign $(-1)^{\delta_{ij}}$ between the amplitudes of one diagram and its counterpart obtained by exchanging the final neutralinos as a result of Fermi statistics. The corresponding matrix element can be written as

$$\begin{aligned}
\mathcal{M} = & \mathcal{M}_s + \mathcal{M}_b + \mathcal{M}_q = \epsilon^\mu(p_1)\epsilon^\nu(p_2)\bar{u}(k_2)P_L \left\{ f_1^L \gamma_\mu \gamma_\nu + f_2^L \gamma_\mu \gamma_\nu \not{p}_1 + f_3^L \gamma_\nu \gamma_\mu + f_4^L \gamma_\nu \gamma_\mu \not{p}_1 \right. \\
& + f_5^L p_{2\mu} \gamma_\nu + f_6^L p_{2\mu} \gamma_\nu \not{p}_1 + f_7^L k_{1\mu} \gamma_\nu + f_8^L k_{1\mu} \gamma_\nu \not{p}_1 + f_9^L p_{1\nu} \gamma_\mu + f_{10}^L p_{1\nu} \gamma_\mu \not{p}_1 + f_{11}^L k_{1\nu} \gamma_\mu \\
& + f_{12}^L k_{1\nu} \gamma_\mu \not{p}_1 + f_{13}^L p_{2\mu} p_{1\nu} + f_{14}^L p_{2\mu} p_{1\nu} \not{p}_1 + f_{15}^L p_{2\mu} k_{1\nu} + f_{16}^L p_{2\mu} k_{1\nu} \not{p}_1 + f_{17}^L k_{1\mu} k_{1\nu} \\
& + f_{18}^L k_{1\mu} k_{1\nu} \not{p}_1 + f_{19}^L k_{1\mu} p_{1\nu} + f_{20}^L k_{1\mu} p_{1\nu} \not{p}_1 + \left. \epsilon_{\mu\nu\alpha\beta} \left[f_{21}^L p_1^\alpha p_2^\beta + f_{22}^L p_1^\alpha p_2^\beta \not{p}_1 \right] \right\} v(k_1) \\
& + (P_L \rightarrow P_R, f_i^L \rightarrow f_i^R). \tag{2.2}
\end{aligned}$$

where $P_{L,R} = \frac{1}{2}(1 \mp \gamma_5)$, $f_k^{L,R}(k = 1, \dots, 22)$ are form factors. \mathcal{M}_s , \mathcal{M}_b and \mathcal{M}_q are the amplitudes of the s-channel, box and quartic interaction diagrams, respectively. Since our calculation shows that the contribution to the cross section is predominantly from s-channel diagrams, we listed the explicit expressions of the form factors for s-channel diagrams in Appendix and omitted the form factor expressions of box and quartic interaction diagrams, because they have long-winded expressions and negligible contribution to cross section in the resonant effect energy region. Then the cross section for this subprocess at one-loop order in unpolarized photon collisions can be obtained by

$$\hat{\sigma}(\hat{s}, \gamma\gamma \rightarrow \tilde{\chi}_i^0 \tilde{\chi}_j^0) = \frac{1}{16\pi \hat{s}^2} \left(\frac{1}{2}\right)^{\delta_{ij}} \int_{\hat{t}^-}^{\hat{t}^+} d\hat{t} \sum_{\bar{}} |\mathcal{M}|^2, \quad (i = 1, j = 1, 2). \tag{2.3}$$

In the above equation, $\hat{t}^\pm = 1/2 \left[(m_{\tilde{\chi}_i}^2 + m_{\tilde{\chi}_j}^2 - \hat{s}) \pm \sqrt{(m_{\tilde{\chi}_i}^2 + m_{\tilde{\chi}_j}^2 - \hat{s})^2 - 4m_{\tilde{\chi}_i}^2 m_{\tilde{\chi}_j}^2} \right]$. The factor $(\frac{1}{2})^{\delta_{ij}}$ is due to the two identical particles in the final states. The bar over the sum means average over initial spins.

The neutralino pair production via photon-photon fusion is only a subprocess of the parent e^+e^- linear collider. The total cross section of the neutralino pair production via photon fusion in e^+e^- collider can be obtained by folding the cross section of the subprocess $\hat{\sigma}(\gamma\gamma \rightarrow \tilde{\chi}_i^0 \tilde{\chi}_j^0)$ with the photon luminosity.

$$\sigma(s) = \int_{(m_{\tilde{\chi}_i} + m_{\tilde{\chi}_j})/\sqrt{s}}^{x_{max}} dz \frac{d\mathcal{L}_{\gamma\gamma}}{dz} \hat{\sigma}(\gamma\gamma \rightarrow \tilde{\chi}_i^0 \tilde{\chi}_j^0) \quad \text{at} \quad \hat{s} = z^2 s, \quad (2.5)$$

where \sqrt{s} and $\sqrt{\hat{s}}$ are the e^+e^- and $\gamma\gamma$ c.m.s. energies respectively and $d\mathcal{L}_{\gamma\gamma}/dz$ is the distribution function of photon luminosity, which is

$$\frac{d\mathcal{L}_{\gamma\gamma}}{dz} = 2z \int_{z^2/x_{max}}^{x_{max}} \frac{dx}{x} f_{\gamma/e}(x) f_{\gamma/e}(z^2/x), \quad (2.6)$$

where $f_{\gamma/e}$ is the photon structure function of the electron beam [14, 15]. We take the structure function of the photon produced by Compton backscattering as [14, 16]

$$f_{\gamma/e}^{Comp}(x) = \begin{cases} \frac{1}{D(\xi)} \left(1 - x + \frac{1}{1-x} - \frac{4x}{\xi(1-x)} + \frac{4x^2}{\xi^2(1-x)^2} \right), & \text{for } x < 0.83, \\ 0, & \text{for } x > 0.83, \end{cases} \quad (2.7)$$

where

$$D(\xi) = \left(1 - \frac{4}{\xi} - \frac{8}{\xi^2} \right) \ln(1 + \xi) + \frac{1}{2} + \frac{8}{\xi} - \frac{1}{2(1 + \xi)^2}, \quad \xi = \frac{4E_0\omega_0}{m_e^2}. \quad (2.8)$$

Taking ω_0 the maximal energy of backscattering photons, or, $\xi = 2(1 + \sqrt{2})$, we have

$$D(\xi) = 1.8397.$$

3. Numerical results and discussions

In this section, we present some numerical results of the total cross section in the mSUGRA scenario from the complete one-loop diagrams for the process $e^+e^- \rightarrow \gamma\gamma \rightarrow \tilde{\chi}_i^0 \tilde{\chi}_j^0$, ($i = 1, j = 1, 2$). The input parameters are chosen as: $m_t = 175 \text{ GeV}$, $m_Z = 91.187 \text{ GeV}$, $m_b = 4.5 \text{ GeV}$, $\sin^2 \theta_W = 0.2315$, and $\alpha = 1/128$. We assume that $\tilde{\chi}_1^0$ is the LSP and escapes detection. In numerical calculation to get the low energy scenario from the mSUGRA, the renormalization group equations(RGE's)[17] are run from the weak scale M_Z up to the GUT scale, taking all thresholds into account. We use two loop RGE's only for the gauge couplings and the one-loop RGE's for the other supersymmetric parameters. The GUT scale boundary conditions are imposed and the RGE's are run back to M_Z , again taking threshold into account.

As we know that the s-channel resonance effects of the intermediate Higgs bosons (see Fig.1(b,c)) could play an important role in some c.m.s. energy regions of incoming photons. With the mSUGRA scenario input parameters used in our numerical calculation, the mass of the lightest Higgs boson h^0 is under the thresholds of W^+W^- and Z^0Z^0 decays. Therefore the relevant decay width of h^0 is mainly contributed by the decay channel of $h^0 \rightarrow b\bar{b}$. The decay channels of H^0 may involve $H^0 \rightarrow q\bar{q}$ (where q may be top and bottom quarks), $H^0 \rightarrow h^0h^0$ (A^0A^0), $H^0 \rightarrow \tilde{\chi}_1^+ \tilde{\chi}_1^-$ ($\tilde{\chi}_i^0 \tilde{\chi}_j^0$ ($i = 1, j = 1, 2$)) and $H^0 \rightarrow W^+W^-$ (Z^0Z^0), if the mass of H^0 is larger than the thresholds of all those decay channels. The main decay channels for the pseudo-scalar Higgs boson are $A^0 \rightarrow Z^0h^0$, $A^0 \rightarrow q\bar{q}$ and $A^0 \rightarrow \tilde{\chi}_1^+ \tilde{\chi}_1^-$ ($\tilde{\chi}_i^0 \tilde{\chi}_j^0$ ($i = 1, j = 1, 2$)) under similar conditions. In our calculation, all the decay widths of the intermediate Higgs

bosons are considered at the tree level and their expressions can be found in appendix B of reference [13].

The cross sections for $\tilde{\chi}_1^0\tilde{\chi}_2^0$ and $\tilde{\chi}_2^0\tilde{\chi}_2^0$ via photon collisions at linear colliders versus the mass of $\tilde{\chi}_2^0$ is shown in Fig.2. The input parameters are chosen as $m_0 = 100 \text{ GeV}$, $A_0 = 300 \text{ GeV}$, $\mu > 0$ and $\tan\beta = 4$. We calculate the cross sections at the collision energies of electron-positron \sqrt{s} being 500 GeV and 1 TeV , respectively. In framework of the mSUGRA, when the mass of $\tilde{\chi}_2^0$ varies from 81 GeV to 251 GeV as shown in Fig.2, chargino mass has the values above the lower limit give in Ref.[7], the masses of Higgs boson H^0 and A^0 increase from 231 GeV to 510 GeV and from 226 GeV to 507 GeV respectively and the mass of the Higgs boson h^0 is always under the threshold of $\tilde{\chi}_1^0\tilde{\chi}_2^0$ decay. Therefore the contribution to the cross section from the s-channel with exchanging h^0 is very small due to the s-channel suppression. The masses of H^0 and A^0 may reach the thresholds of $\tilde{\chi}_1^0\tilde{\chi}_2^0$ and $\tilde{\chi}_2^0\tilde{\chi}_2^0$ decay modes, then the cross section of the subprocess will be strongly enhanced by the s-channel resonant effects when the total energy \sqrt{s} of the subprocess approaches the mass of H^0 or A^0 .

We can see from Fig.2 that all the cross sections for the neutralino pairs $\tilde{\chi}_i^0\tilde{\chi}_j^0$ ($i = 1, 2, j = 1$) decreases with the increment of the value of $m_{\tilde{\chi}_2}$. It can reach 18 femto barn when $\sqrt{s} = 500 \text{ GeV}$ and $m_{\tilde{\chi}_2} \sim 81 \text{ GeV}$. For the two curves of $\sqrt{s} = 500 \text{ GeV}$, the cross sections with $\sqrt{s} = 500 \text{ GeV}$ go down rapidly when the values of the mass of $\tilde{\chi}_2^0$ are in the vicinity of 193 GeV . The reason is that the resonant effects from H^0 and A^0 exchanging s-channels do not contribute to the total cross section, since the maximum c.m.s energy of

incoming photons is $\sqrt{\hat{s}_{max}} \sim 0.83\sqrt{s} < m_{H^0}(m_{A^0})$. That fact reflects that the resonant effect of the s-channels plays an important role in the total cross sections of neutralino pair productions at LC. From this figure we can see that the cross sections of neutralino pair productions with $\sqrt{s} = 500 \text{ GeV}$ are always larger than those with $\sqrt{s} = 1 \text{ TeV}$ when $m_{\tilde{\chi}_2^0}$ is less than 180 GeV , and will be smaller than those with $\sqrt{s} = 1 \text{ TeV}$ when $m_{\tilde{\chi}_2^0}$ is larger than 185 GeV .

In Fig.3 we present the cross sections of neutralino pair productions versus $\tan\beta$ with the colliding energy of electron and positron being 500 GeV and 1 TeV respectively, where the other four input parameters are chosen as $m_0 = 100 \text{ GeV}$, $m_{1/2} = 150 \text{ GeV}$, $A_0 = 300 \text{ GeV}$ and $\mu > 0$. Our calculation in the mSUGRA model shows that when $\tan\beta$ increases from 2 to 32, the mass of $\tilde{\chi}_1^0$ ranges from 51 GeV to 57 GeV and the mass of $\tilde{\chi}_2^0$ ranges from 98 GeV to 102 GeV . So the dependence of the masses of neutralinos on $\tan\beta$ is very weak, but the masses of Higgs boson H^0 and A^0 depend on $\tan\beta$ obviously and decrease from 352 GeV to 166 GeV and from 344 GeV to 165 GeV , respectively. The mass of h^0 is a function of $\tan\beta$ too, but keeps $m_{h^0} < m_{\tilde{\chi}_1^0} + m_{\tilde{\chi}_2^0}$. Since the couplings of Higgs bosons to quarks and squarks pair of the third generation are related to the ratio of the vacuum expectation values, $\tan\beta$ should effect the cross sections substantially due to Yukawa coupling strength. The line shapes in this figure are determined mainly by parts of the form factors of $f_{1,s}^{L,R}$, $f_{13,s}^{L,R}$ and $f_{21,s}^{L,R}$, which come from the diagrams involving couplings between heavy quarks(top or bottom quark) and Higgs bosons. The form factors from these diagrams are all proportional to a factor, which has the form as $\frac{A}{\cos\beta} + \frac{B}{\sin\beta}$. Therefore all the curves in Figure 3 have

similar line shapes. We can see from this figure that the cross section for mixed neutralino pair ($\tilde{\chi}_1^0\tilde{\chi}_2^0$) production is larger than that for diagonal pair($\tilde{\chi}_2^0\tilde{\chi}_2^0$) production. When the ratio of both vacuum expectation values $\tan\beta$ is in the vicinity of $\tan\beta \sim 5$, the cross sections for both $\tilde{\chi}_1^0\tilde{\chi}_2^0$ and $\tilde{\chi}_2^0\tilde{\chi}_2^0$ pair productions can reach maximum, where we have $m_{\tilde{\chi}_1} = 52 \text{ GeV}$ and $m_{\tilde{\chi}_2} = 98 \text{ GeV}$.

4. Summary

In this paper, we studied the pair production processes of the neutralinos via photon-photon fusion at LC. The numerical analysis of their production rates is carried out in the mSUGRA scenario with some typical parameter sets. The results show that the cross section of the neutralino pair productions via photon-photon collisions can reach about 18 femto barn for $\tilde{\chi}_1^0\tilde{\chi}_2^0$ pair production and 9 femto barn for $\tilde{\chi}_2^0\tilde{\chi}_2^0$ pair production at an electro-positron LC operating in $\gamma\gamma$ collision mode with our chosen parameters, which is one order smaller quantitatively than at the machine operating in e^+e^- collision mode. At future TESLA collider, the annual $\gamma\gamma$ luminosity is designed to be $10 - 30 \text{ fb}^{-1}$ and one order higher after upgraded[5], these translate into about $90 \sim 270$ events per year (about 10^3 events after upgrade) for $\tilde{\chi}_2^0\tilde{\chi}_2^0$ production and $180 \sim 540$ events per year (few thousand events after upgrad) for $\tilde{\chi}_1^0\tilde{\chi}_2^0$ production. Our numerical results present a fact that in some c.m.s energy regions of incoming photons, there exist obvious resonance effects from s-channel diagrams by exchanging intermediate H^0 and A^0 Higgs bosons, which can makes observable enhancement on the cross sections of the parent processes at linear colliders.

Acknowledgement: This work was supported in part by the National Natural Science Foundation of China(project number: 19875049), the Youth Science Foundation of the University of Science and Technology of China, a grant from the Education Ministry of China and the State Commission of Science and Technology of China.

Appendix

In this appendix we list the form factors for the one-loop s-channel diagrams. The amplitude of s-channel diagrams, which was defined in Eq.(2.2), has the form

$$\begin{aligned}
\mathcal{M}_s &= \frac{e^2}{16\pi^2} \epsilon^\mu(p_1) \epsilon^\nu(p_2) \bar{u}(k_2) P_L \left\{ f_{1,s}^L \gamma_\mu \gamma_\nu + f_{3,s}^L \gamma_\nu \gamma_\mu + f_{13,s}^L p_{2\mu} p_{1\nu} + f_{21,s}^L \epsilon_{\mu\nu p_1 p_2} \right\} v(k_1) \\
&+ (P_L \rightarrow P_R, f_{k,s}^L \rightarrow f_{k,s}^R) \\
&= \frac{e^2}{16\pi^2} \epsilon^\mu(p_1) \epsilon^\nu(p_2) \bar{u}(k_2) P_L \left\{ 2f_{1,s}^L g_{\mu\nu} + f_{13,s}^L p_{2\mu} p_{1\nu} + f_{21,s}^L \epsilon_{\mu\nu p_1 p_2} \right\} v(k_1) \\
&+ (P_L \rightarrow P_R, f_{k,s}^L \rightarrow f_{k,s}^R),
\end{aligned}$$

where $f_{1,s}^L = f_{3,s}^L$, $f_{1,s}^R = f_{3,s}^R$.

We divide the form factors into four parts: $f_{k,s}^{L(R)} = f_{k,s}^{L(R),W} + f_{k,s}^{L(R),\tilde{\chi}} + f_{k,s}^{L(R),f} + f_{k,s}^{L(R),\tilde{f}}$, which correspond to loop diagrams of W^\pm , charged Higgs bosons and ghost particles in Fig.1(b,4, b.5 and c.3), chargino loops in Fig.1(c.2), quark and lepton loops in Fig.1(c.2), and scalar quark and lepton loops in Fig.1(b.3, c.1) respectively. Notations used in the appendix are defined below,

$$\begin{aligned}
B_{mn}^{1y} &= B_{mn}[-p_1, m_y, m_y], & B_{mn}^{2y} &= B_{mn}[-p_2, m_y, m_y], & B_{mn}^{3y} &= B_{mn}[k_1 + k_2, m_y, m_y], \\
C_{mn}^y &= C_{mn}[-p_2, -p_1, m_y, m_y, m_y],
\end{aligned}$$

$$P_B = \frac{1}{\hat{s} - m_B^2 + im_B \Gamma_B} (B = h^0, H^0, A^0), \quad P_G = \frac{1}{\hat{s} - m_Z^2}.$$

The couplings of Higgs boson(B)- $\tilde{\chi}_j$ - $\tilde{\chi}_i$ ($\tilde{\chi} = \tilde{\chi}^0, \tilde{\chi}^\pm$) are denoted as

$$V_{B\tilde{\chi}_j\tilde{\chi}_i} = V_{B\tilde{\chi}_j\tilde{\chi}_i}^L P_L + V_{B\tilde{\chi}_j\tilde{\chi}_i}^R P_R$$

where $B = h^0, H^0, A^0, G^0$. All the explicit expressions of relevant vertices can be found in the Appendix of [13]. The form factors are expressed explicitly as follows. g represents electroweak coupling constant; Q_f denotes electrical charge ($Q_\tau = -1, Q_t = 2/3$, etc.) and the factor 3 in $f_{k,s}^{f(\tilde{f})}$ arises from quark color.

$$\begin{aligned} f_{1,s}^{L,W} &= P_h \left\{ i[V_{hH^+H^+}(B_0^{3H^+} - 4C_{24}^{H^+}) + V_{hG^+G^+}(B_0^{3W} - m_W^2 C_0^W - 4C_{24}^W)] \right. \\ &+ gm_W \left[-\frac{B_0^{1W} + B_0^{2W}}{2} + (\epsilon - 3)B_0^{3W} + (m_W^2 + 3\hat{s})C_0^W - \frac{\hat{s}}{2}(C_{11}^W + C_{12}^W \right. \\ &+ 2C_{23}^W) + (16 - 5\epsilon)C_{24}^W \left. \right] \sin(\alpha - \beta) \left. \right\} V_{h\tilde{\chi}_j^0\tilde{\chi}_i^0}^L \\ &+ (h^0 \rightarrow H^0, \sin(\alpha - \beta) \rightarrow -\cos(\alpha - \beta)), \end{aligned}$$

$$\begin{aligned} f_{13,s}^{L,W} &= 8i(P_h \{ V_{hH^+H^+}(C_{12}^{H^+} + C_{23}^{H^+}) + V_{hG^+G^+}(C_{12}^W + C_{23}^W) \\ &+ igm_W [2C_0^W + 3(C_{12}^W + C_{23}^W)] \sin(\alpha - \beta) \} V_{h\tilde{\chi}_j^0\tilde{\chi}_i^0}^L \\ &+ (h^0 \rightarrow H^0, \sin(\alpha - \beta) \rightarrow -\cos(\alpha - \beta)), \end{aligned}$$

$$\begin{aligned} f_{1,s}^{L,\tilde{\chi}} &= -i \sum_{x=1}^2 m_{\tilde{\chi}_x^\pm} (2B_0^{1\tilde{\chi}^\pm} - \hat{s}C_0^{\tilde{\chi}^\pm} - 2\hat{s}C_{12}^{\tilde{\chi}^\pm} - 8C_{24}^{\tilde{\chi}^\pm}) \left[P_h V_{h\tilde{\chi}_j^0\tilde{\chi}_i^0}^L (V_{h\tilde{\chi}_x^+\tilde{\chi}_x^-}^L + V_{h\tilde{\chi}_x^+\tilde{\chi}_x^-}^R) \right. \\ &+ (h^0 \rightarrow H^0) + (h^0 \rightarrow A^0) + (h^0 \rightarrow G^0) \left. \right], \end{aligned}$$

$$\begin{aligned} f_{13,s}^{L,\tilde{\chi}} &= -4i \sum_{x=1}^2 [C_0^{\tilde{\chi}^\pm} + 4(C_{12}^{\tilde{\chi}^\pm} + C_{23}^{\tilde{\chi}^\pm})] m_{\tilde{\chi}_x^\pm} \left[P_h V_{h\tilde{\chi}_j^0\tilde{\chi}_i^0}^L (V_{h\tilde{\chi}_x^+\tilde{\chi}_x^-}^L + V_{h\tilde{\chi}_x^+\tilde{\chi}_x^-}^R) \right. \\ &+ (h^0 \rightarrow H^0) + (h^0 \rightarrow A^0) + (h^0 \rightarrow G^0) \left. \right], \end{aligned}$$

$$\begin{aligned}
f_{21,s}^{L,\tilde{\chi}} &= 4 \sum_{x=1}^2 C_0^{\tilde{\chi}^+} m_{\tilde{\chi}^+} \left[P_h V_{h\tilde{\chi}_j^0 \tilde{\chi}_i^0}^L (V_{h\tilde{\chi}_x^+ \tilde{\chi}_x^-}^L - V_{h\tilde{\chi}_x^+ \tilde{\chi}_x^-}^R) + (h^0 \rightarrow H^0) + (h^0 \rightarrow A^0) \right. \\
&\quad \left. + (h^0 \rightarrow G^0) \right], \\
f_{1,s}^{L,f} &= -2iQ_\tau^2 m_\tau (2B_0^{1\tau} - \hat{s}C_0^\tau - 2\hat{s}C_{12}^\tau - 8C_{24}^\tau) (P_h V_{h\tau\tau} V_{h\tilde{\chi}_j^0 \tilde{\chi}_i^0}^L + P_H V_{H\tau\tau} V_{H\tilde{\chi}_j^0 \tilde{\chi}_i^0}^L) \\
&\quad + 3(\tau \rightarrow t) + 3(\tau \rightarrow b), \\
f_{13,s}^{L,f} &= -8iQ_\tau^2 m_\tau [C_0^\tau + 4(C_{12}^\tau + C_{23}^\tau)] (P_h V_{h\tau\tau} V_{h\tilde{\chi}_j^0 \tilde{\chi}_i^0}^L + P_H V_{H\tau\tau} V_{H\tilde{\chi}_j^0 \tilde{\chi}_i^0}^L) \\
&\quad + 3(\tau \rightarrow t) + 3(\tau \rightarrow b), \\
f_{21,s}^{L,f} &= -8m_\tau C_0^\tau (P_A V_{A\tau\tau} V_{A\tilde{\chi}_j^0 \tilde{\chi}_i^0}^L + P_G V_{G\tau\tau} V_{G\tilde{\chi}_j^0 \tilde{\chi}_i^0}^L) + 3(\tau \rightarrow t) + 3(\tau \rightarrow b), \\
f_{1,s}^{L,\tilde{f}} &= iQ_\tau^2 \sum_{x=1}^2 (B_0^{3\tilde{\tau}} - 4C_{24}^{\tilde{\tau}}) (P_h V_{h\tilde{\tau}_x \tilde{\tau}_x} V_{h\tilde{\chi}_j^0 \tilde{\chi}_i^0}^L + P_H V_{H\tilde{\tau}_x \tilde{\tau}_x} V_{H\tilde{\chi}_j^0 \tilde{\chi}_i^0}^L) + 3(\tau \rightarrow t) + 3(\tau \rightarrow b), \\
f_{13,s}^{L,\tilde{f}} &= 8iQ_\tau^2 \sum_{x=1}^2 (C_{12}^{\tilde{\tau}} + C_{23}^{\tilde{\tau}}) (P_h V_{h\tilde{\tau}_x \tilde{\tau}_x} V_{h\tilde{\chi}_j^0 \tilde{\chi}_i^0}^L + P_H V_{H\tilde{\tau}_x \tilde{\tau}_x} V_{H\tilde{\chi}_j^0 \tilde{\chi}_i^0}^L) + 3(\tau \rightarrow t) + 3(\tau \rightarrow b), \\
f_{i,s}^R &= f_{i,s}^L (V_{B\tilde{\chi}_j^0 \tilde{\chi}_i^0}^L \rightarrow V_{B\tilde{\chi}_j^0 \tilde{\chi}_i^0}^R), \quad (i = 1, 13, 21 \quad B = h^0, H^0, A^0, G^0).
\end{aligned}$$

In the above expressions we adopted the definitions of one-loop integral functions in [18] and defined $d = 4 - 2\epsilon$. The numerical calculation of the vector and tensor loop integral functions can be traced back to four scalar loop integrals A_0, B_0, C_0, D_0 as shown in [19].

References

- [1] H.P. Nilles, Phys. Rep. 110(1984) 1; H.E. Haber and G.L. Kane, Phys. Rep. 117(1985) 75.

- [2] R. Davis, et al., Phys. Rev. Lett. **20**, 1205(1968); K. S. Hirata, et al., Phys. Rev. Lett. **65**, 1297(1990); P. Anselmann, et al., Phys. Lett. **B327**, 377(1994); P. Sikivie, in Trends in Astroparticle Physics, Proceeding of the Workshop, Stockholm, Sweden, 1994, edited by L. Bergstrom et al..
- [3] H.E. Haber and G.L. Kane, Phys. Rep. 117(1985)75.
- [4] I.F. Ginzburg, G.L. Kotkin, V.G. Serbo and V.I. Telnov, Pis'ma ZHETF 34 (1981)514; Nucl. Instr. Methods 205 (1983)47.
- [5] R. Brinkmann, G Materlik, J. Rossbach and A. Wagner(Eds), Conceptual Design of a 500 GeV e^+e^- Linear Collider with Integrated X-ray Laser Facility, DESY 1997-048, ECFA 1997-182.
- [6] L3 Collaboration, M. Acciarri et al., Phys. Lett **B472**(2000) 420.
- [7] L3 Collaboration, M. Acciarri et al., Phys. Lett **B482**(2000) 31.
- [8] W. Beenakker, et al., Phys. Rev. Lett. 83 (1999)3780.
- [9] Y. Jiang, W.G. Ma, L. Han, Z.H. Yu and H. Pietschmann, Phys. Rev. **D62** (2000) 034012.
- [10] L. Han, W.G. Ma, Y. Jiang, M.L. Zhou and H. Zhou, Commu. Theor. Phys. 34 (2000) 115.
- [11] G. Moortgat-Pick and H. Fraas, Phys. Rev. **D59**(1998) 015016; G. Moortgat-Pick, A. Bartl, H. Fraas and W. Majerotto, "Exploiting Spin Correlations in Neutralino

- Production and Decay with Polarized e^- and e^+ Beams”, DESY-00-002, UWThPh-2000-3, WUE-ITP-2000-004, HEPHY-PUB 726/2000, hep-ph/0002253.
- [12] M. Drees and S. P. Martin, hep-ph/9504324.
- [13] J. Gunion, H. Haber, G. Kane and S. Dawson, The Higgs Hunter’s Guide (Addison-Wesley, Reading 1990).
- [14] I.F. Ginzburg, G.L. Kotkin, V.G. Serbo and V.I. Telnov, Pis’ma ZHETF 34(1981)514; Nucl. Instr. Methods 205(1983)47.
- [15] R. Blankenbecler and S.D. Drell, Phys. Rev. Lett. 61(2324)1988; F. Halzen, C.S. Kim and M.L. Stong, Phys. Lett. B274(489)1992; M. Drees and R.M. Godbole, Phys. Lett. 67(1189)1991.
- [16] V.Telnov, Nucl. Instr. Methods A294(72)1990.
- [17] V. Barger, M. S. Berger and P. Ohmann, Phys. Rev. **D47**, 1093(1993), **D47**, 2038(1993); V. Barger, M. S. Berger, P. Ohmann and R. J. N. Phillips, Phys. Lett. **B314**, 351(1993); V. Barger, M. S. Berger and P. Ohmann, Phys. Rev. **D49**, 4908(1994).
- [18] Bernd A. Kniehl, Phys. Rep. 240(1994)211.
- [19] G. Passarino and M. Veltman, Nucl. Phys. **B160**, 151(1979).

Figure Captions

Fig.1 The Feynman diagrams of the subprocess $\gamma\gamma \rightarrow \tilde{\chi}_i^0 \tilde{\chi}_j^0$. (a.1 ~ 6) Box diagrams. (b.1 ~ 5) Quartic interaction diagrams. (c.1 ~ 3) Triangle diagrams.

Fig.2 Total cross sections of the process $e^+e^- \rightarrow \gamma\gamma \rightarrow \tilde{\chi}_i^0 \tilde{\chi}_j^0$, ($i = 1, 2, j = 2$) as function of $m_{\tilde{\chi}_{1/2}}$ at electron-positron LC with $\sqrt{s} = 500 \text{ GeV}$. The solid curve and dashed curve are for $\tilde{\chi}_1^0 \tilde{\chi}_2^0$ production at LC with $\sqrt{s} = 500 \text{ GeV}, 1000 \text{ GeV}$, respectively. The dotted curve and dash-dotted curve are for $\tilde{\chi}_2^0 \tilde{\chi}_2^0$ production at LC with $\sqrt{s} = 500 \text{ GeV}$ and 1000 GeV , respectively.

Fig.3 Total cross sections of the process $e^+e^- \rightarrow \gamma\gamma \rightarrow \tilde{\chi}_i^0 \tilde{\chi}_j^0$, ($i = 1, 2, j = 2$) as function of $\tan\beta$. The dashed-lines are for $\tilde{\chi}_2^0 \tilde{\chi}_2^0$ production and the full-line curves are for $\tilde{\chi}_1^0 \tilde{\chi}_2^0$ production, with e^+e^- colliding energy $\sqrt{s} = 500 \text{ GeV}$ and 1000 GeV respectively.

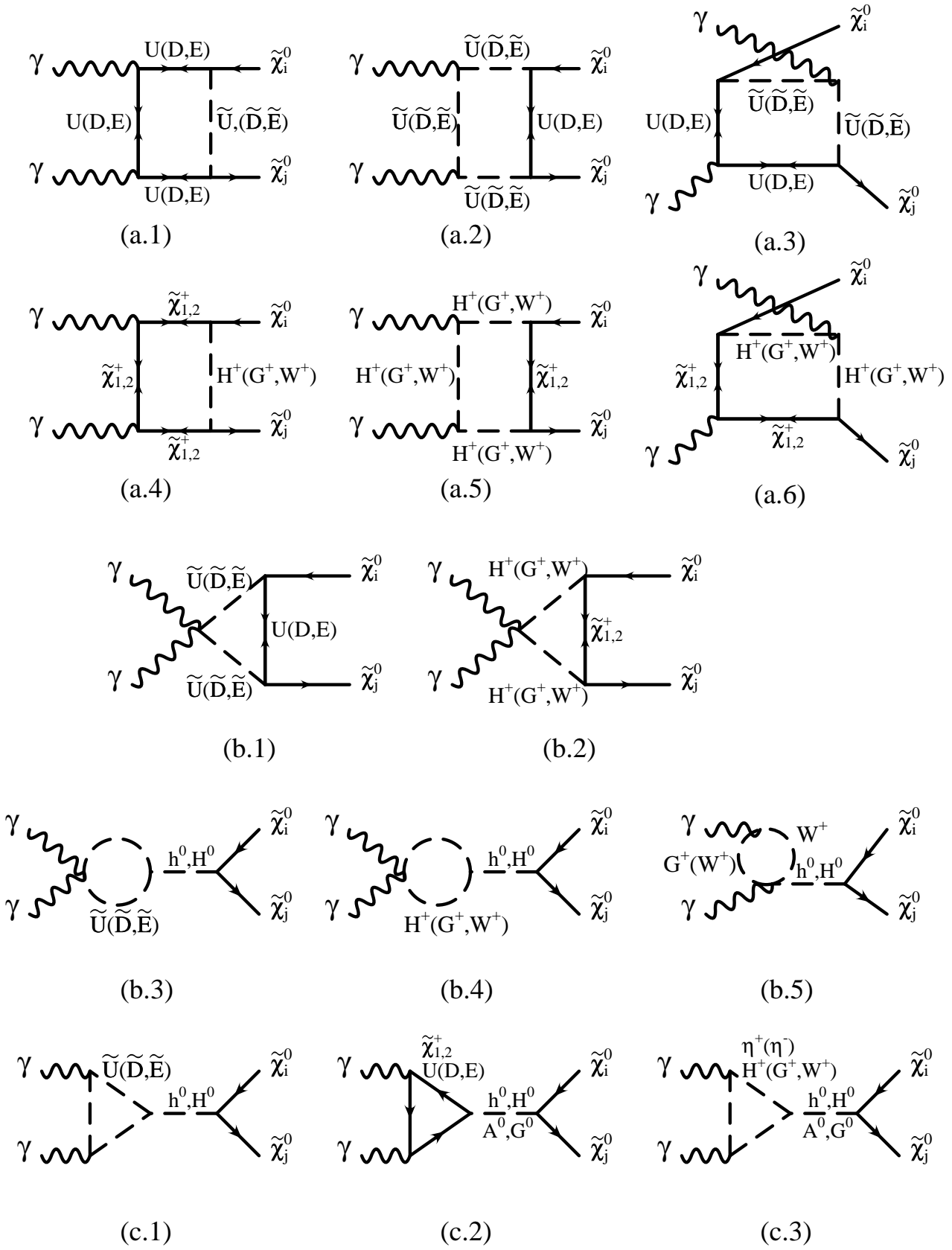


Fig.1

Fig. 2

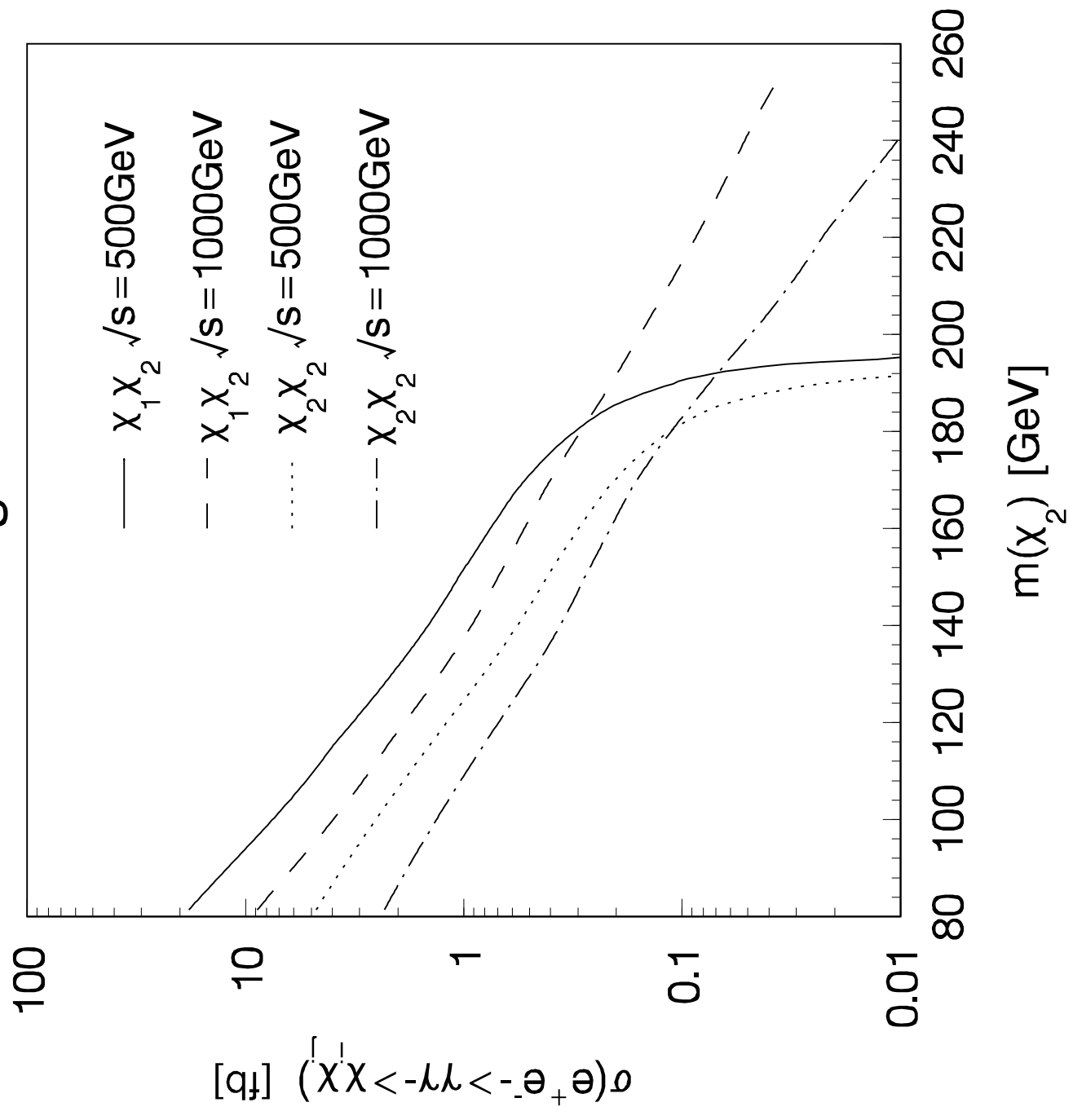


Fig. 3

